Efficient light-driven water oxidation catalysis by dinuclear Ru complexes

Serena Berardi,[a] Laia Francàs,[a] Sven Neudeck,[b] Somnath Maji,[a] Jordi Benet-Buchholz,[a] Franc Meyer[b],* Antoni Llobet[a],*

[a] Dr. S. Berardi, Dr. L. Francàs, Dr. S. Maji, Dr. J. Benet-Buchholz, Prof. Dr. A. Llobet

Institute of Chemical Research of Catalonia (ICIQ)

Av. Països Catalans 16, 43007 Tarragona (Spain)

Fax: (+34) 977920228

www.iciq.org/research/research_group/prof-antoni-llobet/

*allobet@iciq.cat

[b] S. Neudeck, Prof. Dr. F. Meyer

Institute of Inorganic Chemistry, Georg-August-University Göttingen

Tammannstraße 4, 37077 Göttingen (Germany)

Abstract

Mastering the light-induced four electron oxidation of water to molecular oxygen is a key step towards the achievement of the overall water splitting, aimed at producing alternative solar fuels. Following this approach, in this work we report two rugged molecular pyrazolate-based diruthenium complexes, able to efficiently catalyze visible-light-driven water oxidation. These complexes were fully characterized both in the solid state (by means of X-Ray diffraction analysis) and in solution (spectroscopically and electrochemically). Benchmark performances for the homogeneous oxygen production have been obtained for both catalysts in the presence of a photosensitizer and a sacrificial electron acceptor at pH 7, yielding a turnover frequency up to 11.1 s^{-1} and 5300 turnover numbers after 3 successive catalytic runs. In the same experimental conditions and set-up, the pyrazolate-based diruthenium complexes outperform other two well-known water oxidation catalysts, due to both electrochemical and mechanistic aspects.

Introduction

One of the most urgent issues for modern society deals with the increasing global energy demand and the need for sustainable energy supply. The efficient production of clean fuels by the exploitation of renewable energy sources, such as sunlight, is thus highly desirable.[1] The mimicry of natural photosynthesis represents a viable strategy, dealing with the direct conversion and storage of solar energy into chemical bonds.[2] Following this perspective, a challenging approach is offered by photoinduced water splitting into its high-energy constituents (H_2 and O_2, eq. 1),[2,3] with water oxidation (WO, eq. 2) being the bottleneck of the entire process, due to its high thermodynamic and kinetic demands.

$$2\,H_2O \longrightarrow 2\,H_2 + O_2 \qquad (1)$$

$$2\,H_2O \longrightarrow O_2 + 4\,H^+ + 4\,e^- \qquad (E^0 = 1.23\ V\ vs.\ NHE\ at\ pH\ 0) \qquad (2)$$

$$4\,H^+ + 4\,e^- \longrightarrow 2\,H_2 \qquad (E^0 = 0\ V\ vs.\ NHE\ at\ pH\ 0) \qquad (3)$$

Significant efforts have been devoted to the development of efficient water oxidation catalysts (WOCs), both based on metal oxides materials[4,5] or molecular transition metal complexes.[2a,6,7] The latter are particularly useful for unraveling the potential mechanistic pathways for this complex reaction. Indeed, several kinetic investigations, in conjunction with spectroscopic, electrochemical and isotopic labeling experiments as well as DFT calculations, have unraveled a variety of pathways followed in this catalytic reaction.[6-8]

Even though several examples of first row transition metal WOCs have appeared lately,[9] ruthenium complexes are still among the most studied systems in this sense. Following the first pioneering example reported by T. J. Meyer *et al.*,[10] several robust and efficient dinuclear ruthenium WOCs were reported to catalyze oxygen evolution from water with high turnover numbers, in the presence of Ce^{IV} as the sacrificial electron acceptor.[7,11,12] Mononuclear ruthenium complexes were also proposed as WOCs.[13,14] In particular, ruthenium catalysts, featuring 2,2'-bipyridine-6,6'-dicarboxylate (bda) as tetradentate equatorial ligand and substituted isoquinolines as the axial ligands, represents the current benchmark in the chemical WO reaction, yielding a turnover frequencies (TOF) in the range of 1000 s^{-1}, in the presence of large excess of Ce^{IV}.[13b, 14] It is worth noting that for Ru-bda-based complexes, the O-O bond formation step is an intermolecular process involving the interaction of two mononuclear complexes, yielding a dinuclear peroxo species. The formation of the latter is particularly favorable when the π-stacking between the axial isoquinoline ligands can additionally benefit of electronic perturbations arisen from a careful choice of the substituents on the aromatic ring.[14] At the same time, recent results evidenced that some mononuclear monoaqua ruthenium WOCs can be slowly converted by self-assembly into more robust dinuclear complexes, displaying similar catalytic activity towards WO.[15] Although much more challenging from a synthetic point of view, dinuclear complexes can be highly beneficial for the water oxidation process. For the latter, the mechanism of O-O bond formation can be controlled by the relative position of the Ru-O units in addition to the electronic effects exerted by the auxiliary ligands[2,6-8,10,11]. It is worth noting that, in order to be integrated in photocatalytic systems/devices, an attractive WOC must effectively drive not only the chemical

and/or electrochemical water oxidation, but also the corresponding light-driven reaction. The latter is generally performed in a so-called three-component system, including a photosensitizer (as the light-sensitive unit), a sacrificial electron acceptor and the catalyst itself. Optimizing all the processes occurring in the photocatalytic cycle is a challenging task, thus a careful selection of the experimental conditions must be done in order to achieve good results. Among the reported ruthenium WOCs, both mono-[16] and dinuclear [17] complexes, as well as polyoxometalates,[18] have been used various different experimental conditions and O_2 detection set-ups. In a recent example, a remarkable turnover number of 890 has been reported for the photoinduced WO by a carboxybenzoimidazol-pyrazolate-based diruthenium complex.[17a]

Here we present two water soluble and oxidatively rugged diruthenium pyrazolate-based WOCs, able to efficiently photogenerate oxygen from water in the presence of a photosensitizer and a sacrificial electron acceptor, yielding unprecedented results in terms of turnover number (TON) and frequency (TOF). A comparison with two other well-known WOCs in the same experimental conditions is additionally reported, clearly evidencing that the pyrazolate-based diruthenium complexes outperform those previously reported, both for electrochemical and mechanistic reasons.

Results and discussion

Complex **1** (Figure 1) has been recently reported in the literature as a rugged WOC, yielding up to 211 catalytic cycles (TON) at pH 1 in the presence of 1000 eq. of Ce^{IV} as sacrificial electron acceptor.[7] Considering the stoichiometry of WO, a remarkable 84% oxidative efficiency was obtained under these conditions.[7]

Complex **1** displays a *bis*-tridentate monoanionic ligand, namely 4-methyl-*bis*(bipyridyl)pyrazolate ($Mebbp^-$), designed to act as a bridging scaffold, placing the two metal centers in close proximity. The axial positions are occupied by pyridine-3-sulfonate ligands which make the complex highly soluble in aqueous media. The new complex **2** displays the same structural motif as **1**, but bears axial pyridines functionalized with carboxylate units instead of sulfonate moieties. This tailored modification is designed for the further heterogenization of this WOC onto different surfaces, in order to build (photo)anodes for a device capable of artificial photosynthesis. The feasibility of this heterogenization approach has been recently proved, since an analogous diruthenium complex based on $Mebbp^-$ and bearing pyridines with phosphonate groups as the axial ligands has been successfully anchored onto fluorine-doped tin oxide (FTO) electrodes.[19]

It is worth noting, that the presence of the carboxylated pyridines also makes complex **2** fully soluble in aqueous solution, a key feature often lacking in many molecular WOCs. The water solubility allows proper spectroscopic and electrochemical characterization, avoiding the use of organic co-solvents that could affect the already complex kinetics of the WO reaction.[11b]

Complex **2** was synthesized following the strategy depicted in Scheme 1. As reported for the synthesis of complex **1**,[7] $[RuCl_2(dmso)_4]$ was reacted with 2 equivalents of the H-Mebbp ligand in the presence of Et_3N, yielding the complex $[\{Ru^{II}(Cl)(dmso)(H_2O)\}\{Ru^{II}(Cl_2)(dmso)\}(\mu\text{-Mebbp})]$ as synthetic intermediate. Deprotonation of the ligand and its slow addition to $[RuCl_2(dmso)_4]$

are crucial to avoid the formation of complexes in which one metal is coordinated by two $Mebbp^-$ ligands, reminiscent of grid-like structures, previously reported for this type of pyrazolate ligands.[20] The intermediate was further reacted in the presence of an excess of pyridine-4-carboxylic acid in a 1:1 MeOH:H_2O solution containing Na_2CO_3, affording the sodium salt of the μ-CO_3 bridged complex $[\{Ru^{II}(py\text{-}COO)_2\}_2(\mu\text{-}Mebbp)(\mu\text{-}CO_3)]^{3-}$ (**2**(CO_3)) in 23% isolated yield. Since the removal of exogenous bridging ligands from this kind of complexes is not always straightforward,[7] it is worth mentioning that in the case of complex **2**(CO_3) the carbonate bridge can be removed by stirring in pH 0-1 triflic acid solution or sonicating in pH 7 phosphate buffer, yielding the catalytically active *bis*-aquo species **2** (*cfr.* Scheme 2 and electrochemical characterization in the text).

The solid state structure of the sodium salt of complex **2**(CO_3) was elucidated by means of X-ray diffraction analysis. As shown in Figure 2a, the coordination sphere of the two ruthenium centers is slightly distorted from octahedral. While the *bis*-meridional $Mebbp^-$ ligand is almost planar and both ruthenium ions are located almost within the pyrazolate plane (RuNNRu torsion angle = 2.6°), the bridging carbonate that occupies the remaining equatorial positions of the two ruthenium ions is not coplanar, but severely twisted with respect to the RuNNRu plane (NRuOC torsion angle = 32.7°). This twisting may evidence that the Ru···Ru distance in **2**(CO_3) is not ideal for hosting the exogenous carbonate, which may explain its straightforward removal upon acidification/sonication. The axial positions in **2**(CO_3) are occupied by four monodentate carboxylated pyridines, two of which are facing each other and can interact *via* π-stacking (the distance between the pyridine-N atoms N9 and N10 is 3.6 Å), while the other two are rotated with respect to each other. Furthermore, the peripheral carboxylic moieties interact with the Na^+ cations, resulting in a cluster stabilized by methanol molecules. This cluster connects the **2**(CO_3) molecules with each other to give a polymeric arrangement in the crystal lattice (Figures 2b and S1a). The overall 3D packing shows randomly distributed cavities (one of them shown in Figure S1b), in which methanol molecules can be accommodated.

Complex **2**(CO_3) was also fully characterized in solution by means of both 1D and 2D NMR spectroscopy (Figures 3 and S2-S6) which evidences the diamagnetic character of the low-spin d^6 Ru(II) ions. All resonances could be unambiguously assigned, and the complex showed apparent C_{2v} symmetry on the NMR time scale. These data confirm that the molecular structure of **2**(CO_3) found in solid state is retained in solution, but rotation of the axial pyridines and the toggling of the bridging carbonate are facile processes.

Electrochemical analysis of this kind of complexes is pivotal for the full understanding of their redox properties at the operational pH. Thus, apart from the characterization of novel complex **2** at pH 7, a deeper electrochemical investigation, by means of cyclic voltammetry (CV) and differential pulse voltammetry (DPV), was also performed for complex **1**, in an extended pH range (0-9) with respect to previous reports (0-1.5).[7]

It is worth noting, that the potential displacement of aquo ligands from the Ru centres by coordinating anions has been already pointed out for other diruthenium WOCs.[11b,12] It is likely to happen also in the case of complex **1**, in particular if electrochemical experiments are conducted in buffers with high anion loading such as phosphate buffers. The produced anated species displays a different electrochemical behaviour than **1**, thus complicating a proper electrochemical characterization of the latter. On the other hand, the anation of the labile

aquo positions has been reported to be strongly reduced when this kind of complexes are in oxidation states higher then II,II.[7,11b] In view of this, the reported electrochemical characterization of **1** has been performed starting from the one electron oxidized $Ru^{III}Ru^{II}$ complex, obtained by means of bulk electrolysis. As shown in Figure 4a, an electrochemically reversible oxidation wave was observed at 0.49 V *vs.* NHE in phosphate buffer at pH 7, followed by an electrochemically quasi-reversible 2-electrons wave at 0.85 V *vs.* NHE. When scanning up to higher oxidation potentials (Figure 4b), the catalytic WO wave was observed, at an onset potential of 1.45 V *vs.* NHE. In this case, the second wave becomes electrochemically irreversible, likely because of the slow kinetics of the associated process, while the first one shows full reversibility, thus excluding the decomposition of **1**.

The assignment of all the redox processes involved, including the proton content of each species, was established by means of a Pourbaix diagram (Figure 5). From the analysis of this plot and the calculated slopes, the electrochemical processes observed at pH 7 are the following (eqs. 4-7):

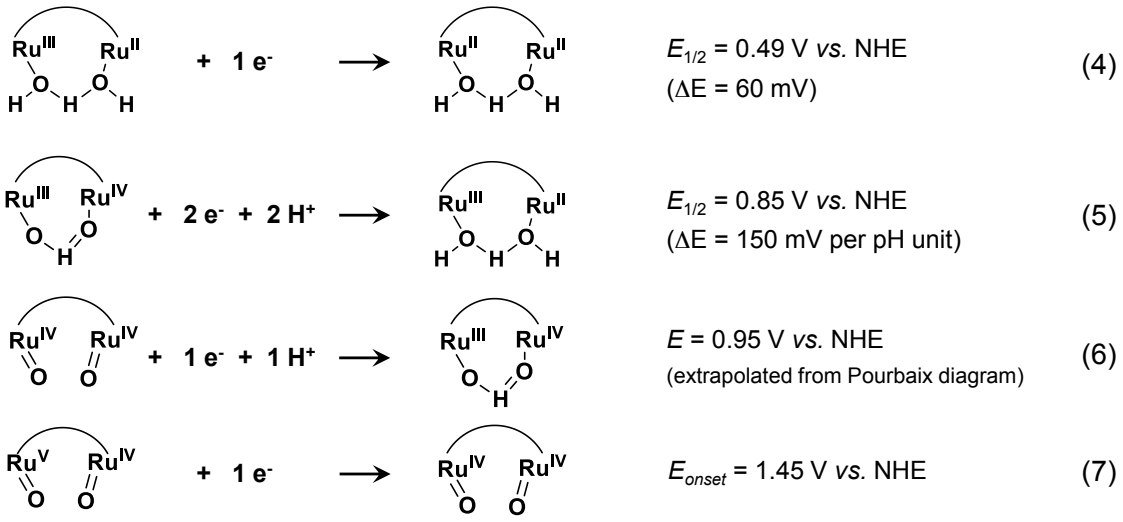

The *E* value for the proton coupled electron transfer process yielding the $Ru^{IV}(O)Ru^{IV}(O)$ species (eq. 6) has been extrapolated from the Pourbaix diagram, since it could not be experimentally observed in the whole pH range, as already reported for similar compounds.[21]

Once the $Ru^{V}(O)Ru^{IV}(O)$ species is formed, catalytic water oxidation takes place, as indicated by an intense electrocatalytic wave (E_{onset} = 1.45 V *vs.* NHE at pH 7).

The electrochemical characterization of complex **2** in phosphate buffer at pH 7 (Figure S7) shows two electrochemically quasi-reversible processes at 0.59 and 0.88 V *vs.* NHE, before the catalytic WO onset at 1.48 V *vs.* NHE. The moderately higher potential of the first wave for **2** with respect to **1** can be ascribed to the effect exerted by the carboxylated pyridines *vs.* the sulphonated ones. On the other hand, the second process and the WO onset remain almost unaffected by the different substituents on the axial pyridines.

Analysis of the electrochemical properties of complexes **1** and **2** at pH 7 clearly shows the need of a highly oxidizing dye in order to drive the light induced water oxidation in the presence of

persulfate as the sacrificial electron acceptor. A functionalized ruthenium *tris*-bipyridyl dye (namely **P2** in Figure 1, displaying two 4,4'-bis(ethoxycarbonyl)-2,2'-bipyridines) was thus synthesized following literature procedures.[22] Since the presence of Cl^- anions was previously reported to decrease the amount of photoproduced O_2,[16a] PF_6^- counteranions were selected to isolate the dye. The measured redox potential of **P2** is 1.62 V *vs.* NHE in phosphate buffer at pH 7 (Figure S14), which is 0.36 V higher than the non-functionalized **P1** ($E_{1/2,\mathbf{P1}}$ = 1.26 V *vs.* NHE). Most importantly, its redox potential is 0.17 V higher than the electrocatalytic wave observed for **1** (0.14 V higher in case of **2**), thus enabling the formation of the catalytically active species for the proposed WOCs.

The efficiency of **1** and **2** as catalysts for the photodriven water oxidation was evaluated in 25 mM phosphate buffer at pH 7, using **P2** as the photosensitizer and sodium persulfate as the sacrificial electron acceptor. RuPS-$S_2O_8^{2-}$ systems are widely used to investigate the photoinduced WO, and have been reported to follow the well-established cycle shown in Scheme 2.[23]

Irradiation was performed by a Xe Arc Lamp (400 nm cut-off filter) and the oxygen evolution was monitored in the liquid phase using a Clark-type electrode in a reactor specifically designed to avoid headspace (Hansatech Instruments). The results of are collected in Table 1. All the four components (light, catalyst, dye and sacrificial electron acceptor) are needed to yield significant amounts of O_2 (see entries 1 and 2 in Table 1 and Figure S15). As already mentioned, the oxidizing power of the dye is actually a key parameter in this system, since when using **P1** as the photosensitizer, O_2 photoproduction is almost negligible (entry 6 in Table 1).

In the presence of **P2**, the proposed catalytic system shows unprecedented performances in terms of O_2 evolution in the presence of very small amounts of WOCs **1** or **2** (0.4 nmol, entries 3 and 4 in Table 1 and Figure 6). In the case of the first cycle catalyzed by complex **1**, up to 935 nmol of O_2 were photoproduced, almost saturating the solution. The resulting turnover numbers (TONs) and turnover frequencies (TOFs) are, to our knowledge, the highest reported so far (up to 2373 and 11.1 s^{-1}, respectively). It is worth noting, that the excited state of RuPS dyes is known to be quenched by O_2, thus hindering the oxidant generation step (see Scheme 2). In our set-up, this aspect is pivotal since the photoproduced O_2 is retained in solution (no headspace available). Thus, we were delighted to observe that the catalytic activity of the proposed system can be restored by only degassing the reaction mixture. In fact, bubbling N_2 in the reaction mixture and restarting the irradiation, yielded up to 3 runs of O_2 production (Figure 7 and Table 1, entry 4, results in parentheses), with unprecedented total TONs up to 5300.

WOC concentration can be further lowered (to 6 x 10^{-8} M, see entry 5 in Table 1 for complex **1**), still giving interesting results in terms of both turnover numbers (up to 2810) and frequency (7.9 s^{-1}). Even in this case, a second catalytic run can be performed after degassing the reaction mixture with N_2 (see Figure S13 and Table 1, entry 5, results in parentheses), yielding a remarkable total TON of 4256.

At this point it is worth mentioning that in this kind of photocatalytic systems, the limiting factors that eventually stop the O_2 evolution are usually the degradation of the dye due to

nucleophilic attacks onto the ligands[24] and the pH drop due to the stoichiometry of the water oxidation reaction itself. Indeed, after the abovementioned 2 or 3 WO runs by **1**, both a decrease of the pH (down to 3.6-4.0) and a change in the UV-vis spectra of the reaction mixture (Figure S14) were observed. In particular, the bleaching of the characteristic absorption band of the dye at about 490 nm is ascribable to decomposition of the dye. Successive attempts of basifying the solution with NaOH to pH 7 and of adding more dye and sacrificial electron acceptor, were not successful in restoring the catalytic activity of the reaction mixture. However, it is interesting to note that in our conditions, even after the addition of another aliquot of **1**, O_2 evolution was not observed, thus indicating some kind of inhibition of the photocatalytic system after the first runs rather than a decomposition of the catalyst itself. This inhibition could be caused by the increased ionic strength of the medium (sulfate ions are produced during the catalysis, see Scheme 2), which has previously been reported to negatively affect the performances of this kind of systems by reducing the quenching efficiency of the RuPS excited state by persulfate.[16a] Furthermore, highly concentrated buffers/ionic media can hinder the coordination of water to complex **1** in its lower oxidation state, and thus the WO catalysis, due to the abovementioned competing anation process by phosphate or sulfate ions. This hypothesis has been indirectly evidenced by a photocatalytic experiment in which 0.1 M sodium sulfate was added to the 25 mM phosphate buffer medium. In this case, a > 30% abatement in the O_2 photoproduction by **1** was observed after the first illumination run (TON = 1580).

It is worth pointing out, that a comparison of the performances of different WOCs is pivotal in the evaluation of the efficiency of novel catalytic systems. However, a direct comparison with literature values is usually difficult, since the reported reaction conditions and set-ups are often very different. To this end, we synthesized two well-known WOCs, *viz*. the dinuclear $[Ru_2(\mu\text{-OAc})(bpp)(trpy)_2]$ (bpp: *bis*-(2-pyridyl)-3,5-pyrazolate; trpy: 2,2':6',2''-terpyridine, complex **3** in Figure 1)[11a] and the mononuclear $[Ru(bda)(pic)_2]$ (bda: 2,2'-bipyridine-6,6'-dicarboxylate; pic: picoline, complex **4** in Figure 1),[13a] in order to directly compare their activity under the same conditions and experimental set-up as **1** and **2**. As shown in Table 1 (entries 3 and 4 *vs.* 7 and 8) and in Figure 6, **1** and **2** clearly outperform the other two WOCs. In the case of complex **3**, the catalytic onset for WO at pH 7 is at 1.60 V *vs.* NHE (Figure S15), which is close to the potential of the dye ($E_{1/2,\mathbf{P1}}$ = 1.62 V *vs.* NHE). Thus the catalysis in the proposed experimental system is slowed down and only small amounts of photoproduced oxygen are obtained (entry 7, Table 1). On the other hand, mononuclear complex **4** is reported to catalyze WO already at 0.98 V *vs.* NHE in phosphate buffer at pH 7.[16e] The observed differences in the efficiency of water oxidation for **1** and **2** with respect to **4** can be related to their different mechanisms. For **1**, an O-O bond formation step involving a water nucleophilic attack has been reported,[7] while for complex **4** the intermolecular coupling of two ruthenium oxo moieties occurs in order to form the dimeric peroxo species.[13a] The µM concentration range generally used for these experiments seriously reduces reactions rates for WOCs whose rate determining step (rds) is bimolecular with respect to [Ru], as is the case of **4**, as compared with catalysts whose rds is unimolecular with respect to [Ru], as is the case of **1-3**. Furthermore, the electron transfer kinetics from the catalyst to the dye can also influence the overall generation of dioxygen.

Another key parameter to be assessed when evaluating the performances of a photochemical reaction is the quantum yield ϕ, *i.e.* the amount of photoproduced O_2 per absorbed photon. In RuPS-$S_2O_8^{2-}$ systems, the limiting value that can be reached for this parameter is 0.5, since two photons are needed to produce one O_2 molecule (the sulfate radical, generated after the quenching of the excited state of RuPS by $S_2O_8^{2-}$, is in fact responsible for the thermal oxidation of a second RuPS molecule)[16a,23b]. The ϕ values, reported in Table 1, were calculated at the initial 100 s of irradiation (provided by a white light source calibrated to 100 mW cm^{-2}), *i.e.* when O_2 production is linear (see also SI). For the proposed catalytic systems, quantum yields up to 0.048 were obtained with complex **1**, again outperforming the other tested WOCs.

Conclusions

In conclusion, we have reported two molecular diruthenium complexes based on the $Mebbp^-$ ligand framework (**1** and **2**) that efficiently catalyze the photoinduced water oxidation at neutral pH in a RuPS-$S_2O_8^{2-}$-type system. To our knowledge, the obtained results represent a new benchmark for the homogeneous light-induced water oxidation, yielding the highest TONs (up to 5300) and TOFs (up to 11.1 s^{-1}) in subsequent catalytic runs. Two well-known literature complexes, **3** and **4**, which partly show better performances in chemically induced WO, have been investigated under identical conditions. Indeed, the new complexes **1** and **2** were shown to outperform **3** and **4** in the photoinduced WO. Heterogenization strategies aimed at covalently anchoring **2** onto the surface of metal oxides are currently under investigation in order to build a (photo)anode based on this promising system.

Experimental Section

Materials

Pyridine-4-carboxylic acid (99%), $Na_2S_2O_8$ (99%), Na_2SO_4 (≥ 99%), Na_2CO_3 (≥ 99%), NaH_2PO_4 (99%) and Na_2HPO_4 (98%) were purchased from Sigma-Aldrich and used without further purification. 25 mM phosphate buffer pH 7 was prepared dissolving the proper amounts of NaH_2PO_4 and Na_2HPO_4 in high purity deionized water, obtained with an UltraClear water purifier system (SG Wasseraufbereitung und Regeneration GmbH).

Syntheses

$[Ru^{II}(bpyCO_2Et)_2(bpy)](PF_6)_2$,[22] $Na[\{Ru^{II}(py\text{-}SO_3)_2(H_2O)\}_2(\mu\text{-}Mebbp)]$ (complex **1**)[7] and synthetic intermediate $[\{Ru^{II}(Cl)(dmso)(H_2O)\}\{Ru^{II}(Cl_2)(dmso)\}(\mu\text{-}Mebbp)]$[7] were synthesized according to literature procedures.

Synthesis of $Na_3[\{Ru^{II}(py\text{-}COO)_2\}_2(\mu\text{-}Mebbp)(\mu\text{-}CO_3)]$, complex 2($CO_3$)

$[\{Ru^{II}(Cl)(dmso)(H_2O)\}\{Ru^{II}(Cl_2)(dmso)\}(\mu\text{-}Mebbp)]$ was synthesized according to literature procedures.[7] 78.5 mg of this complex (0.09 mmol, 1.0 eq) and Na_2CO_3 (30.7 mg, 0.29 mmol, 3.2 eq) were suspended in a degassed 1:1 MeOH/H_2O mixture (5 mL) and refluxed for 3 h.

Thereafter, 88.6 mg of pyridine-4-carboxylic acid (0.72 mmol, 8.0 eq) were added and the mixture heated to reflux overnight. After evaporation of the solvents, the obtained solid was washed with acetone and with a small portion of cold water, before being redissolved in the minimum amount of MeOH. After the addition of Et_2O to this solution, the brown precipitate (complex **2**(CO_3) was filtered and finally dried under reduced pressure. Isolated yield: 23% (25.4 mg, 0.021 mmol).

^{1}H NMR (500.13 MHz, D_2O, 25°C): δ = 9.33 (br s, COOH), 8.62 (d, *J* = 5.8 Hz, 2 H, H13), 8.13 (d, *J* = 8.0 Hz, 2 H, H5), 7.99 (d, *J* = 8.6 Hz, 2 H, H10), 7.89 (d, *J* = 7.9 Hz, 2 H, H7), 7.84 (d, *J* = 6.4 Hz, 8 H, H4'), 7.82 (t, *J* = 7.1 Hz, 2 H, H11), 7.75 – 7.73 (m, 2 H, H12), 7.72 (t, *J* = 8.0 Hz, 2 H, H6), 6.94 (d, *J* = 6.6 Hz, 8 H, H3'), 3.13 (s, 3 H, H1) ppm. ^{13}C{^{1}H} NMR (125.85 MHz, D_2O, 25°C): δ = 173.4 (bridging $\underline{C}O_3^{2-}$), 171.3 (C1'), 163.3 (C2'), 161.0 (free $\underline{C}O_3^{2-}$), 158.7 (C4), 151.9 (C4'), 149.1 (C13), 148.9 (C3), 145.2 (C9), 142.6 (C8), 136.4 (C11), 132.3 (C6), 123.0 (C12), 122.7 (C3'), 122.2 (C10), 121.1 (C2), 118.8 (C5), 117.8 (C7), 9.2 (C1) ppm. UV-Vis (c = 3.78 x 10^{-5} M in 25 mM phosphate buffer pH 7); λ [nm] (ε [L $mol^{-1}cm^{-1}$]): 258 (1.2 x 10^4), 306 (9.6 x 10^3), 380 (1.1 x 10^4), 409 (1.1 x 10^4), 537 (sh, 1.7 x 10^3). ESI-MS (MeOH:H_2O = 1:1) *m/z* : pos: 1145.1 [**2**(CO_3) + 4xH]$^+$; 595.0 [**2**(CO_3) + 2xNa + 3xH]$^{2+}$; neg: 1187 [**2**(CO_3) + 2xNa]$^-$; 1165 [**2**(CO_3) + 1xH + 1xNa]$^-$; 1143 [**2**(CO_3) + 2xH]$^-$. EChem: $E_{1/2}$ (1 mM of **2**(CO_3) in 25 mM phosphate buffer pH 7. After sonication, WOC **2** is formed) [V *vs.* NHE]: 0.59, 0.88, 1.43 (see Figure S7 and main text for assignment).

Instrumentation and Measurements

NMR Spectra were recorded on an Avance 500 (Bruker) instrument in D_2O, with residual protons as internal references. UV-Vis spectra were collected using a Varian Cary-50 Bio spectrophotometer. Cyclic Voltammetry (CV), Differential Pulse Voltammetry (DPV) and Square-Wave Voltammetry (SWV) experiments were performed either on CH-660 and CH-620 potentiostat (CH Instruments, *Inc.*) as well as on a Model 263A (PerkinElmer). A glassy carbon disk (diameter = 2 mm) was used as the working electrode, a platinum disk or wire as the auxiliary, and $Hg/Hg_2SO_4/K_2SO_4$ *sat.* or Saturated Calomel Electrode (SCE) as the reference. The glassy carbon disk electrode was polished with 0.05 μm alumina paste and all electrodes were washed with water and dried before use. All pH values were measured with a HI 4222 pH meter (Hanna Instruments) using a calibrated Crison 5029 electrode (Crison Instruments) or with a 780M pH meter (Metrohm) using an Ecotrode Plus (Metrohm) pH electrode.

Photoinduced water oxidation experiments

Photoinduced water oxidation experiments were performed in a specific dark chamber (Hansatech Instruments), displaying an integrated Clark-type electrode able to measure the produced oxygen in the liquid-phase (no headspace is left in this kind of experiments). Before each experiment, the oxygen sensor was calibrated at both the fully air- and nitrogen-saturated solution. In a typical experiment, $[Ru^{II}(bpyCO_2Et)_2(bpy)](PF_6)_2$ (0.2 mM) and $Na_2S_2O_8$ (10 mM) were dissolved in 25 mM phosphate buffer pH 7 and introduced in the dark chamber (total volume = 2 mL), thermostated at 25.0°C. The proper amount of catalyst (0.1-0.4 nmol) was then added, the solution stirred and degassed, and the chamber finally closed with a screw cap equipped with a septum. After calibration and baseline collection, the solution was irradiated by opening the windows of the chamber. The illumination was provided by a 150 W

Xe Arc Lamp (LS-150, ABET technology), equipped with a <400 nm filter and calibrated to 1 sun (100 mW/cm^2) using a calibrated silicon photodiode.

X-ray structure determination

Crystals of Na_3[**2**(CO_3)]·8.33(MeOH) were obtained by slow diffusion of diethyl ether into a solution of complex **2**(CO_3) in methanol. The measured crystals were prepared under inert conditions immersed in perfluoropolyether as protecting oil for manipulation.

Data collection: Crystal structure determination for Na_3[**2**(CO_3)]·8.33(MeOH) was carried out using a Apex DUO Kappa 4-axis goniometer equipped with an APPEX 2 4K CCD area detector, a Microfocus Source E025 IuS using MoK_α radiation, Quazar MX multilayer Optics as monochromator and an Oxford Cryosystems low temperature device Cryostream 700 plus (*T* = -173 °C). Full-sphere data collection was used with *ω* and φ scans. Programs used: Data collection APEX-2,[25] data reduction Bruker Saint[26] V/.60A and absorption correction SADABS.[27]

Structure Solution and Refinement: Crystal structure solution was achieved using direct methods as implemented in SHELXTL[28] and visualized using the program XP. Missing atoms were subsequently located from difference Fourier synthesis and added to the atom list. Least-squares refinement on F^2 using all measured intensities was carried out using the program SHELXTL. All non hydrogen atoms were refined including anisotropic displacement parameters.

Comments to the structure of Na_3[**2**(CO_3)]·8.33(MeOH): The asymmetric unit contains one molecule of the metal complex, three sodium atoms and 8 1/3 methanol molecules. The sodium atoms form a cluster of six sodium atoms which are attached to eight carboxylic acid anions. The methanol molecules are disordered in 12 positions. CCDC 1058563 contains the supplementary crystallographic data for this paper. These data can be obtained free of charge from the Cambridge Crystallographic Data Centre via www.ccdc.cam.ac.uk/data_request/cif.

Acknowledgements

MINECO (CTQ-2013-49075-R and Severo Ochoa Excellence Accreditation 2014-2018 (SEV-2013-0319), AGAUR (2014 SGR 915), the DFG (project Me 1313/9-1) and “La Caixa” foundation are gratefully acknowledged. S.B. is grateful to the ICIQ-IPMP Marie Curie COFUND Project (291787ICIQ-IPMP) and S.N. is grateful for a fellowship within the PhD program Catalysis for Sustainable Synthesis (CaSuS).

Keywords: artificial photosynthesis · dinuclear ruthenium complexes · photoinduced water oxidation · redox chemistry · water splitting

Table 1. Overview of the performance of catalyst **1** and **2** together with literature known **3** and **4** in photoinduced water oxidation catalysis in the presence of photosensitizer **P1** or **P2** and $Na_2S_2O_8$ as sacrificial electron acceptor. The O_2 evolution was measured in the **liquid phase**.

Entry	WOC	RuPS	E_{onset} *vs.* NHE [V][a]	Total O_2 [nmol]	TON[b]	TOF_i[c] [s^{-1}]	Quantum yield ϕ[d]
1	---	**P2**	---	0	---	---	---
2	**2**	---	---	7	< 15	---	---
3	**2**	**P2**	1.48	926[e]	2362[e]	9.2	0.041
4	**1**	**P2**	1.45	935[e] (2180[f])	2373[e] (5300[f])	11.1	0.048
5[g]	**1**	**P2**	---	340[e] (515[h])	2810[e] (4256[h])	7.9	0.012
6	**1**	**P1**	---	6	< 15	0.02	---
7	**3**	**P2**	1.60	27	67	0.13; 0.29[i]	0.001
8[j]	**4**	**P2**	0.98	159[e] (260[h])	405[e] (662[h])	0.36; 0.99[i]	0.018

Reaction conditions: 2 x 10^{-7} M WOC; 10^{-2} M $Na_2S_2O_8$; 2 x 10^{-4} M RuPS in 25 mM phosphate buffer pH 7 (2 mL). Irradiation provided by a 150 W Xe lamp equipped with a 400 nm cut-off filter and calibrated to 1 sun (100 mW cm^{-2}). T = 25°C. [a] $E_{1/2,\ \mathbf{P1}}$ = 1.26 V *vs.* NHE and $E_{1/2,\ \mathbf{P2}}$ = 1.62 V *vs.* NHE. [b] TON was calculated as the total amount of O_2 per mole of WOC. [c] Initial TOF, calculated from the linearly fitted O_2 evolution plots in the first 60 s of irradiation. [d] ϕ was calculated as reported in the SI. [e] 1st cycle of O_2 photogeneration, average values of 2-3 replicates. [f] In parentheses, total O_2 production and TON after 3 cycles, only degassing with N_2 between one cycle and the following (see also Figure 7). [g] 6 x 10^{-8} M WOC. [h] In parentheses, total O_2 production and TON after 2 cycles, only degassing with N_2 between one cycle and the following. [i] Calculated after the observed induction time of *ca.* 100 s. [j] Introduced as acetonitrile solution (1% of the total volume).

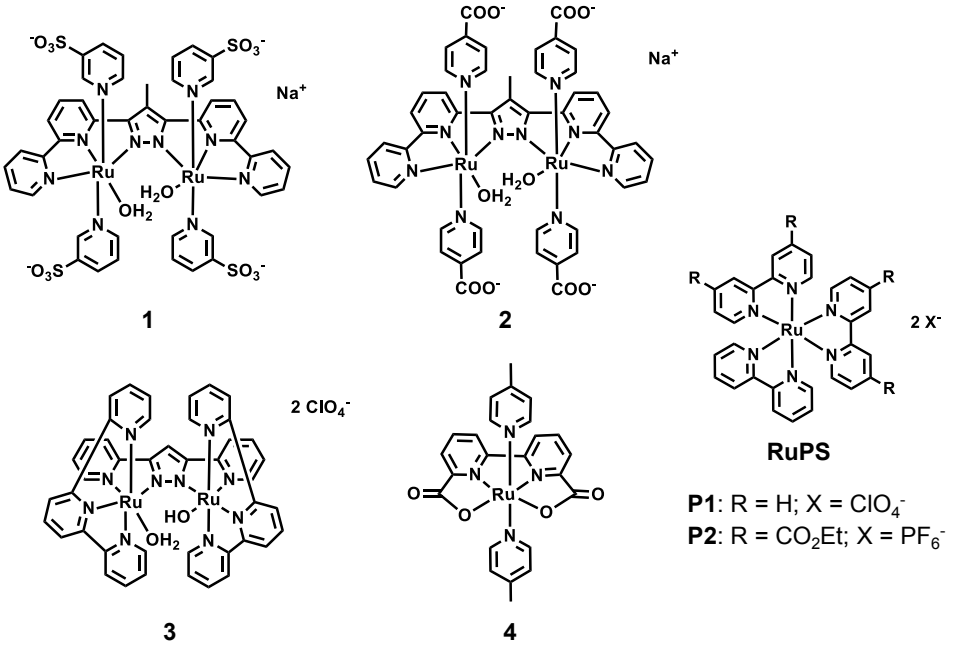

Figure 1. Structures of WOCs and dyes (RuPS) used in this work.

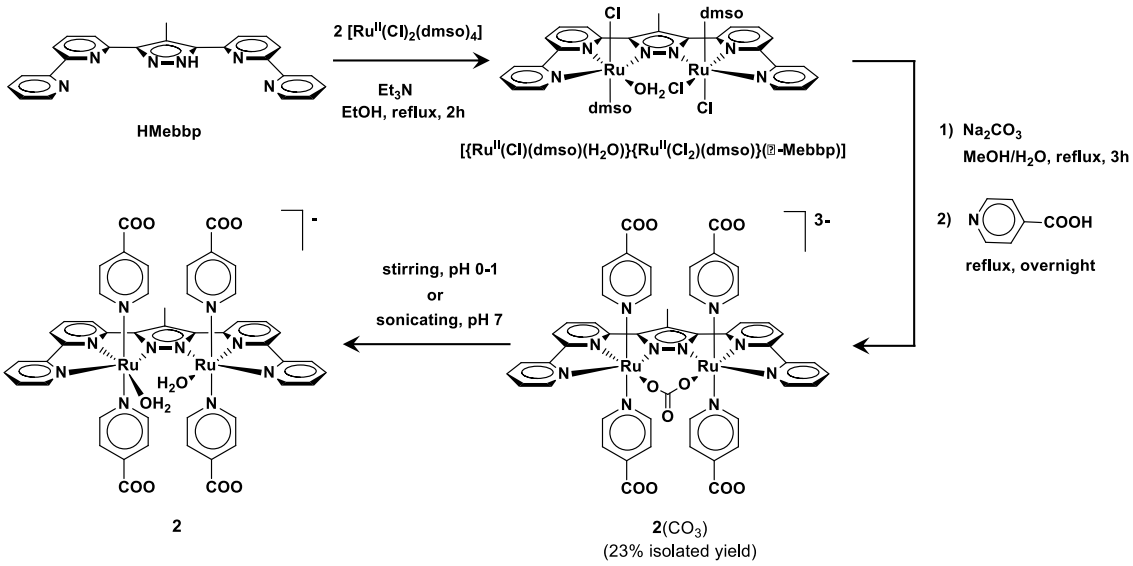

Scheme 1. Synthesis of complex **2**.

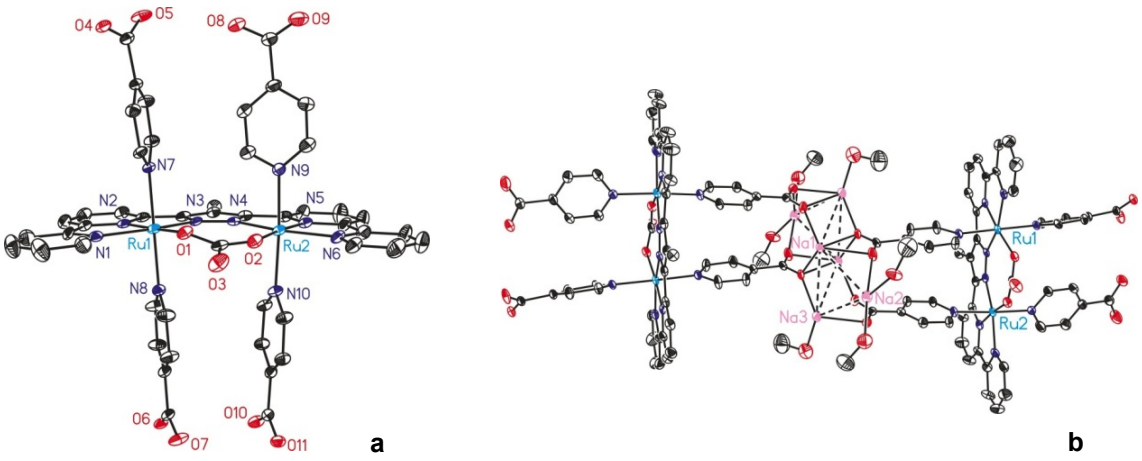

Figure 2. a) ORTEP plot (50% probability) of the anionic Ru complex **2**(CO_3). b) ORTEP plot (50% probability) showing the Na^+ cluster connecting two molecules of **2**(CO_3). Hydrogen atoms, additional counterions and solvent molecules have been omitted to improve clarity.

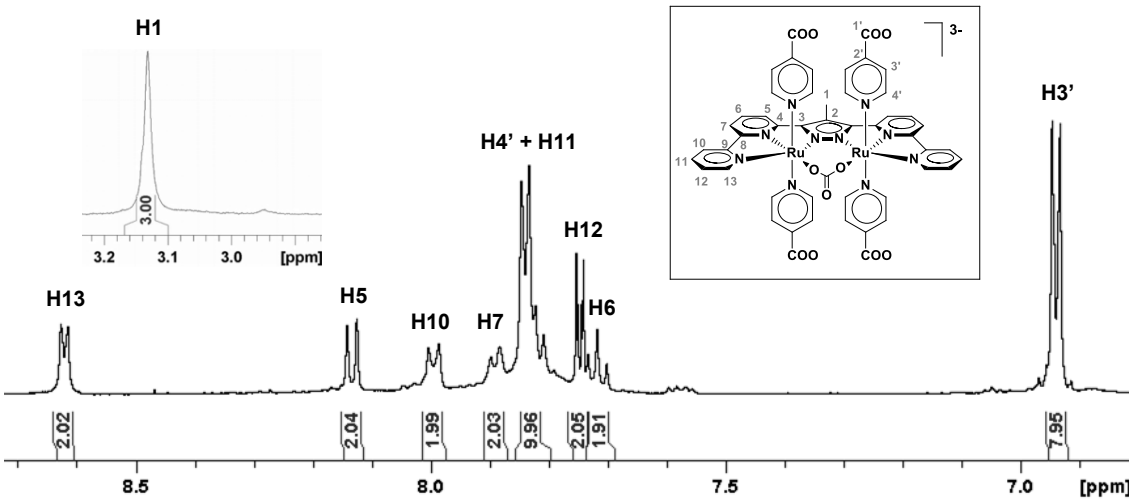

Figure 3. ^{1}H NMR spectrum (500.13 MHz) of complex **2**(CO_3) in D_2O in the chemical shift range 6.8-8.7 ppm. Insets: Expansion of the 2.9-3.2 ppm range and labelling scheme for the assignment of all the resonances (deduced by both 1D and 2D spectra).

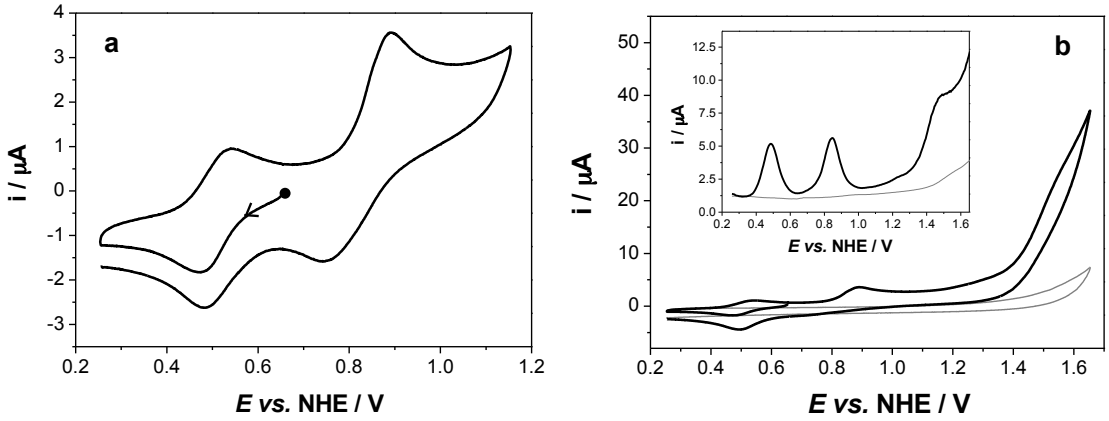

Figure 4. a) CV of 0.5 mM complex **1** in phosphate buffer at pH 7 (total ionic strength = 0.1 M). Scan rate: 0.1 V s^{-1}. b) CV and DPV of 0.5 mM complex **1** (black traces) in phosphate buffer at pH 7 (total ionic strength = 0.1 M) showing the WO catalysis. Gray traces: blank measurements of electrolytic solution. CV: Scan rate = 0.1 V s^{-1}. DPV: Incr. = 0.004 V, Amplitude = 0.05 V, Pulse Width = 0.05 s, Sample Width = 0.0167 s, Pulse period = 0.5 s. Working electrode: glassy carbon disk (diameter = 2 mm); counter electrode: platinum disk; reference electrode: $Hg/Hg_2SO_4/K_2SO_4$ *sat*.

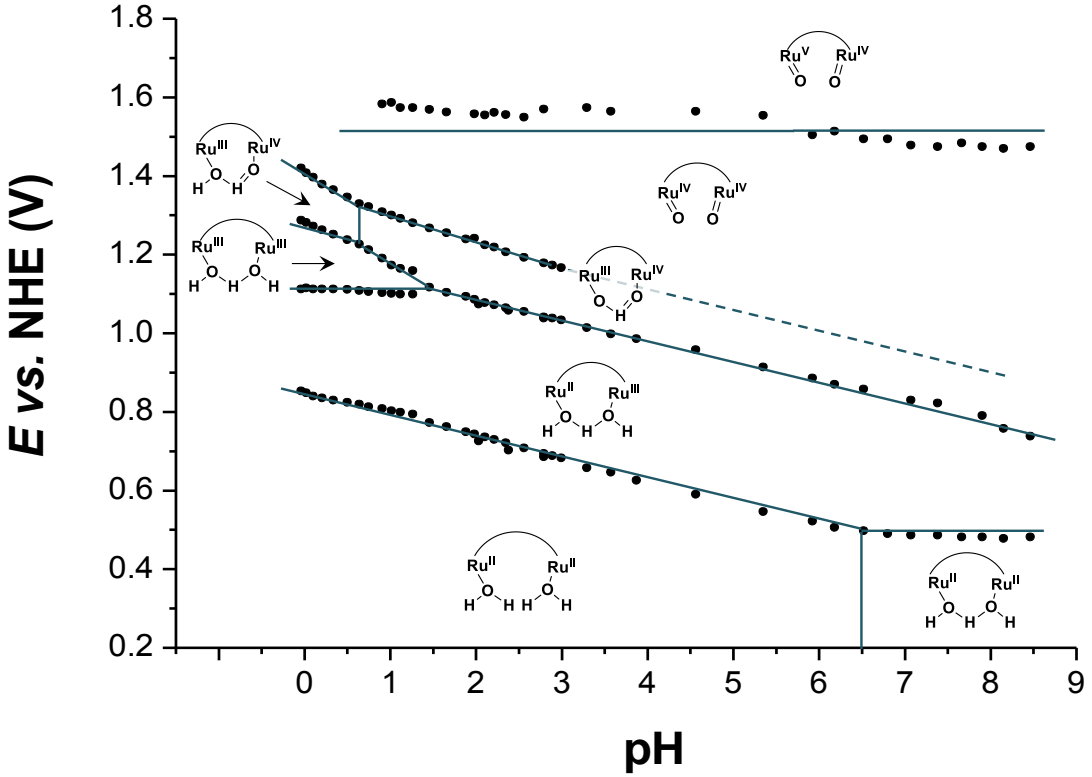

Figure 5. Pourbaix diagram of complex **1**, obtained from CV experiments collected at different pHs. The process indicated by the dashed line could not be experimentally observed above pH 3.

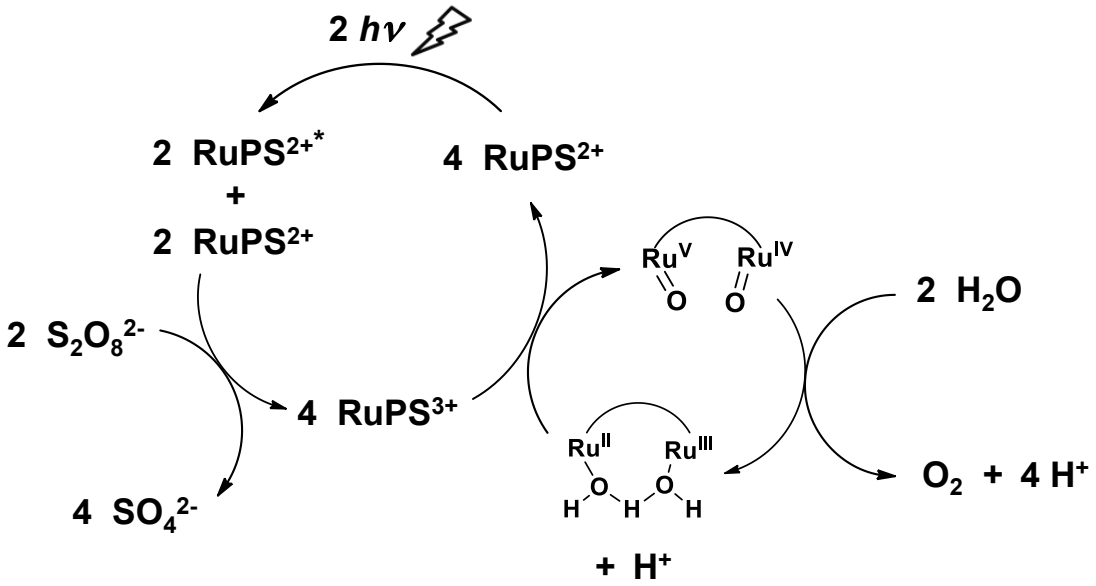

Scheme 2. General scheme for the processes occurring during the photodriven water oxidation in the presence of a ruthenium *tris*-bipyridyl-type dye (RuPS), $S_2O_8^{2-}$ as the sacrificial electron acceptor and complex **1** as the WOC. The stoichiometry of the reactions account for the fact that the sulfate radical, generated after the quenching of the excited state of RuPS by $S_2O_8^{2-}$, is responsible for the thermal oxidation of a second RuPS molecule.

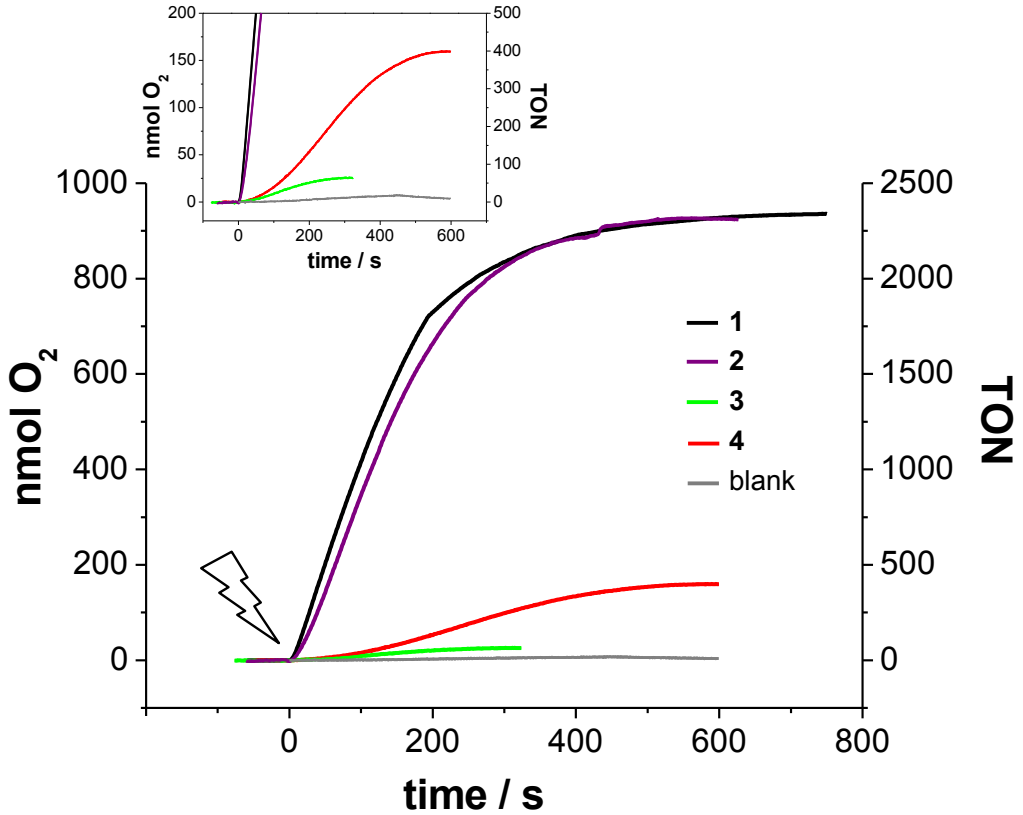

Figure 6. Photocatalytic oxygen production by the investigated WOCs. Reaction conditions: 2 x 10^{-7} M WOC; 10^{-2} M $Na_2S_2O_8$; 2 x 10^{-4} M RuPS in 25 mM phosphate buffer pH 7 (2 mL). Irradiation provided by a 150 W Xe lamp equipped with a 400 nm cut-off filter and calibrated to 1 sun (100 mW cm^{-2}). *T* = 25°C. Inset: Expanded graph in the 0-200 nmol O_2 (0-500 TON) range. Flashes: light on.

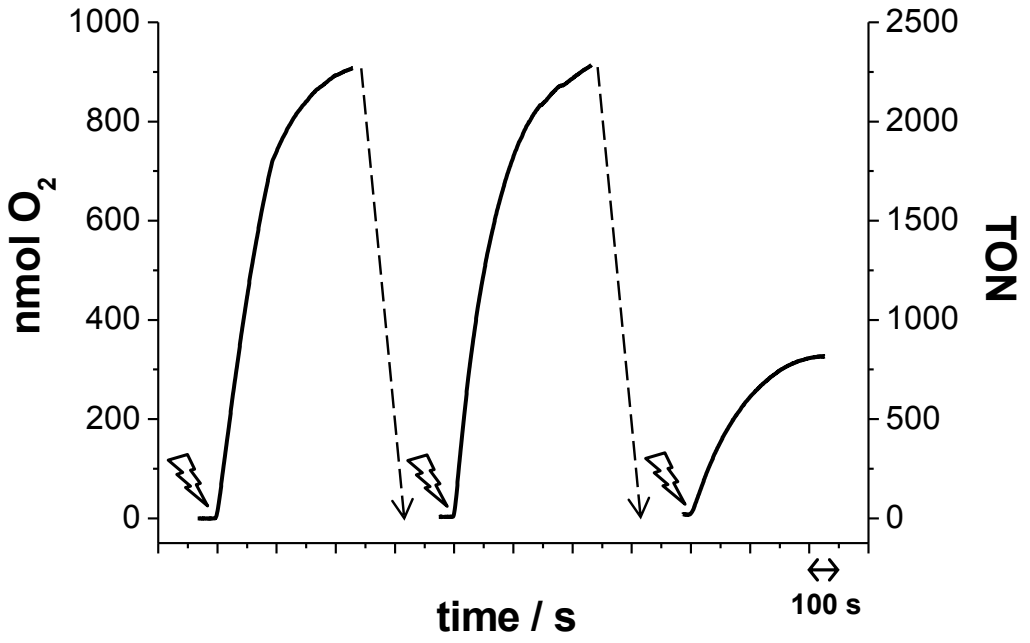

Figure 7. Photocatalytic oxygen production by **1** in subsequent runs. Reaction conditions: 2 x 10^{-7} M **1**; 10^{-2} M $Na_2S_2O_8$; 2 x 10^{-4} M **P2** in 25 mM phosphate buffer pH 7 (2 mL). Irradiation provided by a Xe lamp equipped with a 400 nm cut-off filter and calibrated to 1 sun (100 mW cm^{-2}). *T* = 25°C. Dashed arrows: degassing the reaction mixture with N_2. Flashes: light on.

References

[1] N. S. Lewis, D. G. Nocera *Proc. Natl. Acad. Sci. U. S. A.* **2006**, *103*, 15729-15735.

[2] a) S. Berardi, S. Drouet, L. Francàs, C. Gimbert-Suriñach, M. Guttentag, C. J. Richmond, T. Stoll, A. Llobet *Chem. Soc. Rev.* **2014**, *43*, 7501-7519; b) J. Barber *Chem. Soc. Rev.* **2009**, *38*, 185-196.

[3] Y. Tachibana, L. Vayssieres, J. R. Durrant *Nat. Photonics* **2012**, *6*, 511-518.

[4] F. E. Osterloh *Chem. Soc. Rev.* **2013**, *42*, 2294-2320.

[5] X. Chen, C. Li, M. Graetzel, R. Kostecki, S. S. Mao *Chem. Soc. Rev.* **2012**, *41*, 7909-7937.

[6] R. Bofill, J. García-Antón, L. Escriche, X. Sala, A. Llobet in *Comprehensive Inorganic Chemistry II*, (Eds. J. Reedijk and K. Poeppelmeier), Elsevier, Amsterdam, 2nd edn, **2013**, pp. 505-523.

[7] S. Neudeck, S. Maji, I. López, S. Meyer, F. Meyer, A. Llobet *J. Am. Chem. Soc.* **2014**, *136*, 24-27.

[8] X. Sala, S. Maji, R. Bofill, J. García-Antón, L. Escriche, A. Llobet *Acc. Chem. Res.*, **2014**, *47*, 504-516.

[9] a) M. L. Rigsby, S. Mandal, W. Nam, L. C. Spencer, A. Llobet, S. S. Stahl *Chem. Sci.* **2012**, *3*, 3058-3062; b) E. A. Karlsson, B.-L. Lee, T. Åkermark, E. V. Johnston, M. D. Kärkäs, J. Sun, Ö. Hansson, J.-E. Bäckvall, B. Åkermark *Angew. Chem.* **2011**, *123*, 11919-11922; *Angew. Chem. Int. Ed.* **2011**, *50*, 11715-11718; c) S. M. Barnett, K. I. Goldberg, J. M. Mayer *Nat. Chem.* **2012**, *4*, 498-502; d) M.-T. Zhang, Z. Chen, P. Kang, T. J. Meyer *J. Am. Chem. Soc.* **2013**, *135*, 2048-2051.

[10] S. W. Gersten, G. J. Samuels, T. J. Meyer *J. Am. Chem. Soc.* **1982**, *104*, 4029-4030.

[11] a) C. Sens, I. Romero, M. Rodríguez, A. Llobet, T. Parella, J. Benet-Buchholz *J. Am. Chem. Soc.* **2004**, *126*, 7798-7799; b) F. Bozoglian, S. Romain, M. Z. Ertem, T. K. Todorova, C. Sens, J. Mola, M. Rodríguez, I. Romero, J. Benet-Buchholz, X. Fontrodona, C. J. Cramer, L. Gagliardi, A. Llobet *J. Am. Chem. Soc.* **2009**, *131*, 15176-15187.

[12] A. C. Sander, S. Maji, L. Francàs, T. Böhnisch, S. Dechert, A. Llobet, F. Meyer *ChemSusChem* DOI: 10.1002/cssc.201403344.

[13] a) L. Duan, F. Bozoglian, S. Mandal, B. Stewart, T. Privalov, A. Llobet, L. Sun *Nat. Chem.* **2012**, *4*, 418-423; b) L. Wang, L. Duan, Y. Wang, M. S. G. Ahlquist, L. Sun *Chem. Commun.* **2014**, *50*, 12947-12950.

[14] C. J. Richmond, R. Matheu, A. Poater, L. Falivene, J. Benet-Buchholz, X. Sala, L. Cavallo, A. Llobet *Chem. Eur. J.* **2014**, *20*, 17282-17286.

[15] I. López, M. Z. Ertem, S. Maji, J. Benet-Buchholz, A. Keidel, U. Kuhlmann, P. Hildebrandt, C. J. Cramer, V. S. Batista, A. Llobet *Angew. Chem.* **2014**, *126*, 209-213; *Angew. Chem. Int. Ed.* **2014**, *53*, 205-209.

[16] a) A. Lewandowska-Andralojc, D. E. Polyansky, R. Zong, R. P. Thummel, E. Fujita *Phys. Chem. Chem. Phys.* **2013**, *15*, 14058-14068; b) S. Roeser, P. Farràs, F. Bozoglian, M. Martínez-Belmonte, J. Benet-Buchholz, A. Llobet *ChemSusChem* **2011**, *4*, 197-207; c) N. Kaveevivitchai, R. Chitta, R. Zong, M. El Ojaimi, R. P. Thummel *J. Am. Chem. Soc.* **2012**, *134*, 10721-10724; d) L. Duan, Y. Xu, M. Gorlov, L. Tong, S. Andersson, L. Sun *Chem. Eur. J.* **2010**, *16*, 4659-4668; e) L. Duan, Y. Xu, P. Zhang, M. Wang, L. Sun *Inorg. Chem.* **2010**, *49*, 209-215; f) L. Duan, Y. Xu, L. Tong, L. Sun *ChemSusChem* **2011**, *4*, 238-244; g) L. Tong, Y. Wang, L. Duan, Y. Xu, X. Cheng, A. Fischer, M. S. G. Ahlquist, L. Sun *Inorg. Chem.* **2012**, 51, 3388-3398; h) L. Wang, L. Duan, L. Tong, L. Sun *J. Catal.* **2013**, *306*, 129-132.

[17] a) T. M. Laine, M. D. Kärkäs, R.-Z. Liao, T. Åkermark, B.-L. Lee, E. A. Karlsson, P. E. M. Siegbahn, B. Åkermark *Chem. Commun.* **2015**, *51*, 1862-1865; b) Y. Xu, A. Fischer, L. Duan, L. Tong, E. Gabrielsson, B. Åkermark, L. Sun *Angew. Chem.* **2010**, *122*, 9118-9121; *Angew. Chem. Int. Ed.* **2010**, *49*, 8934-8937; c) Y. Xu, L. Duan, L. Tong, B. Åkermark, L. Sun *Chem. Commun.* **2010**, *46*, 6506-6508.

[18] a) F. Puntoriero, G. La Ganga, A. Sartorel, M. Carraro, G. Scorrano, M. Bonchio, S. Campagna *Chem. Commun.* **2010**, *46*, 4725-4727; b) Y. V. Geletii, Z. Huang, Y. Hou, D. G. Musaev, T. Lian, C. L. Hill *J. Am. Chem. Soc.* **2009**, *131*, 7522-7523; c) C. Besson, Z. Huang, Y. V. Geletii, S. Lense, K. I. Hardcastle, D. G. Musaev, T. Lian, A. Proust, C. L. Hill *Chem. Commun.* **2010**, *46*, 2784-2786; d) P.-E. Car, M. Guttentag, K. K. Baldridge, R. Alberto, G. R. Patzke *Green Chem.* **2012**, *14*, 1680-1688.

[19] L. Francàs, L. Schaaf, S. Neudeck, S. Maji, J. Benet-Buchholz, F. Meyer, A. Llobet, *submitted.*

[20] a) J. I. Van der Vlugt, S. Demeshko, S. Dechert, F. Meyer *Inorg. Chem.* **2008**, *47*, 1576-1585; b) B. Schneider, S. Demeshko, S. Dechert, F. Meyer *Angew. Chem.* **2010**, *122*, 9461-9464; *Angew. Chem. Int.*

Ed. **2010**, *49*, 9274-9277; c) B. Schneider, S. Demeshko, S. Neudeck, S. Dechert, F. Meyer *Inorg. Chem.* **2013**, *52*, 13230-13237.
[21] A. Llobet, P. Doppelt, T. J. Meyer *Inorg. Chem.* **1988**, *27*, 514-520.
[22] B. H. Farnum, J. J. Jou, G. J. Meyer *Proc. Natl. Acad. Sci. U. S. A.* **2012**, *109*, 15628-15633.
[23] a) H. S. White, W. G. Becker, A. J. Bard *J. Phys. Chem.* **1984**, *88*, 1840-1846; b) K. Henbest, P. Douglas, M. S. Garley, A. Mills *J. Photochem. Photobiol. A: Chem.* **1994**, *80*, 299-305.
[24] P. K. Ghosh, B. S. Brunschwig, M. Chou, C. Creutz, N. Sutin *J. Am. Chem. Soc.* **1984**, *106*, 4772-4783.
[25] Data collection with APEX II versions v2009.1-02 and v2013.4-1. Bruker (2007). Bruker AXS Inc., Madison, Wisconsin, USA.
[26] Data reduction with Bruker SAINT versions V7.60A and V8.30c. Bruker (2007). Bruker AXS Inc., Madison, Wisconsin, USA.
[27] SADABS: V2008/1 and V2012/1 Bruker (2001). Bruker AXS Inc., Madison, Wisconsin, USA. Blessing, *Acta Cryst.* **1995**, *A51*, 33-38.
[28] G. M. Sheldrick *Acta Cryst.* **2008**, *A64*, 112-122. SHELXTL version V6.14.